Chaos and Structures in Rotating Convection at Finite Prandtl Number

Y. Ponty,[1] T. Passot,[1,2] and P. L. Sulem[1]
[1]*CNRS, UMR 6529, Observatoire de la Côte d'Azur, B.P. 4229, 06304 Nice Cedex 4, France*
[2]*Arizona Center for Mathematical Sciences, Department of Mathematics, University of Arizona, Tucson, Arizona 85721*
(Received 15 March 1996; revised manuscript received 24 March 1997)

It is shown, using a generalized Swift-Hohenberg equation, that a small rotation inhibits the spiral chaos which develops in Rayleigh-Bénard convection at moderate Prandtl number. This is due to the gliding and gradual annihilation of dislocations. For rigid top and bottom boundary conditions, a slow rotation first breaks the chiral symmetry and if sufficient leads to an unfolding of the spirals. This effect is maximum near the critical rotation for the onset of the Küppers-Lortz instability, and, when the horizontal geometry is periodic, straight rolls may even reform. With free-slip boundaries, these structures are subject to a small-angle instability, which leads to the formation of large coherent targets embedded in a turbulence background. [S0031-9007(97)03542-4]

PACS numbers: 47.52.+j, 47.20.Lz, 47.27.Te, 47.54.+r

Thermal convection in a Boussinesq fluid with high Prandtl number P, rotating around a vertical axis is known to develop spatiotemporal chaos, when the Taylor number $T_a = \tau^2$ is larger than a critical value [1]. This dynamics results from the Küppers-Lortz (KL) instability [2,3] which destabilizes straight parallel rolls as soon as the Rayleigh number R exceeds the convection threshold R_c. It leads to the formation of patches of straight rolls penetrating each other in a chaotic way: rolls disappear and are replaced by other rolls tilted by an angle θ_{KL} close to 58°.

At moderate Prandtl number (assuming $P > 0.67$ to avoid overstability), the KL instability survives, but the angle θ_{KL} associated with the most unstable mode decreases with the Prandtl number, both for rigid [4,5] and free-slip top and bottom boundaries [6]. In the latter case (often used in the context of astro- and geophysical flows), the usual perturbation method used to analyze the KL instability near convection threshold leads to a divergence in the small angle limit [5]. This reflects the existence of an additional and stronger instability present in a small-angle boundary layer [6]. This "small-angle instability" develops whatever the value of the rotation rate and can be viewed as the continuation of the skewed-varicose instability which destabilizes critical rolls near onset in the absence of rotation [7]. At small enough Prandtl number (below $P \approx 5$), the KL and the small-angle instabilities cannot be separated as a result of the decrease of θ_{KL} and the enhancement of the unstable small-angle range when P is reduced.

Whereas for infinite Prandtl number, the KL dynamics can be qualitatively reproduced by a set of three amplitude equations [8], the description of the dynamics at moderate Prandtl numbers, where θ_{KL} is significantly smaller than 60° ($\theta_{\mathrm{KL}} = 38.4°$ for $P = 0.8$), requires Swift-Hohenberg type equations reproducing the correct variation of the KL instability with the Prandtl number. Such a model was recently derived by a perturbation expansion near threshold [9]. In the case of free-slip top and bottom boundaries, it is obtained by a simplification of a systematically derived set of equations for the leading vertical velocity mode W and the (horizontal) mean flow potential Ψ. In the case of no-slip boundaries, the mean flow equation together with the linear part of the equation for the convective mode is exactly derived by projection of the mean flow on the vertical mode $\sin \pi z$ ($0 < z < 1$) and of the vertical velocity on the first eigenmode of the fourth derivative operator with appropriate boundary conditions [10]. The nonlinear couplings arising in the equation for W are selected among those present in the free-slip case, with coefficients adjusted in such a way that the correct boundary of the zigzag instability in the absence of rotation, and the right critical rotation and most unstable angle θ_{KL} for the KL instability be reproduced. Denoting by ϵ the normalized distance from threshold, the system reads

$$\tau_0 \partial_t W = [\epsilon - (\Delta + 1)^2]W - \mathcal{N}(W, \Psi), \quad (1)$$

$$[\partial_t - P(\nu + \Delta)]\Delta\Psi = (\nabla\Delta W \times \nabla W) \cdot \hat{\mathbf{z}} + \alpha_6[(\Delta W)^2 + \nabla W \cdot \nabla \Delta W] + \alpha_7 \Delta(W^2), \quad (2)$$

with $\mathcal{M} = W^2 + |\nabla W|^2$ and

$$\mathcal{N}(W, \Psi) = \mathcal{M} W + \alpha_1 \nabla W \cdot \nabla \mathcal{M} + \alpha_2(\nabla W \times \nabla \mathcal{M}) \cdot \hat{\mathbf{z}} \alpha_3 (\nabla W \times \nabla \Psi) \cdot \hat{\mathbf{z}} + \alpha_4 W \Delta \Psi + \alpha_5 \nabla W \cdot \nabla \Delta \Psi .$$

In the case of free-slip boundaries, $\nu = \alpha_7 = 0$. Moreover, in the absence of rotation, the coefficients α_2, α_4, α_5, and α_6 vanish, and the model generalizes the equations obtained by Manneville [11] by the inclusion of an additional coupling. For rigid boundaries, $\alpha_4 = \alpha_5 = 0$. Furthermore, the friction coefficient ν is found to be $\nu = \pi^2/q_c^2$ (where q_c denotes the critical wave number) and thus decreases as the rotation rate is increased. Note the presence of the additional term $\alpha_7 \Delta(W^2)$ in the mean flow equation,

originating from the vertical Reynolds stress. A related although less elaborated model was independently presented in [12].

Because of the small-angle instability arising at moderate Prandtl number when free-slip boundary conditions are prescribed, the nonlinear dynamics developing in this case is expected to be significantly different from that obtained with rigid boundaries, and the two situations are to be discussed separately.

In the simpler case of no-slip boundaries, simulations were performed both in a periodic geometry and in a cylindrical box, a configuration best suited for comparison with laboratory experiments. In the periodic case, we used a standard Fourier pseudospectral method with resolutions of 128^2 or 256^2 collocation points, according to the aspect ratio Γ which measures the number of rolls in the convection cell. In the presence of lateral boundaries, compact finite differences were used in the radial direction and a Fourier decomposition performed for the angular variable, with a resolution of 91×240 grid points for about 16 rolls within the box. To avoid the constraint of very small time steps, the unnecessary high resolution near the center of the box was reduced by retaining a number of nonzero angular Fourier modes decreasing with the distance to the center. A random noise with a spectrum localized in an annulus centered around the critical wave number was used as initial conditions.

We first report on the case of a periodic geometry. In the absence of rotation, for a moderate value of the Prandtl number ($P = 1.2$) and a large enough value of the stress parameter ($\epsilon = 0.7$), the now well documented spiral turbulence state [13–19] develops. The mean flow, resulting from roll curvature gradients, consists mostly in large-scale circulation between the structures. Vanishing exactly for perfect targets, it is small in the center of the spirals that it advects in clockwise or anticlockwise rotating motions, depending on the sign of the dislocation imprisoned in the center of the structure.

As seen in Fig. 1, with a small rotation, spirals rotating in the direction of the external rotation are progressively selected, as in the laboratory experiments [20]. This effect is due to the formation of vorticity patches in the center of targets and spirals, whose sign is that of the rotation, as can be seen from the mean flow equation.

As the Rossby number is increased, the spirals grow in size while their number is reduced [Figs. 2(a) and 2(b)]. Near a critical value τ_c, the pattern evolves to almost straight rolls swept by gliding dislocations [Fig. 2(c)] which gradually annihilate by collisions (see also [21]). An analysis of the defect dynamics in the infinite Prandtl number limit is presented in [22]. The ratio $\tau_c/\tau_{\mathrm{KL}}$ (where τ_{KL} denotes the critical rotation for the onset of the Küppers-Lortz instability) grows as the Prandtl number decreases. Its value is close to unity for Prandtl numbers exceeding a few units and approaches 2 for $P = 0.8$. When the rotation rate is larger than τ_c, the KL instability is sufficient to destabilize the structure and leads to the usual

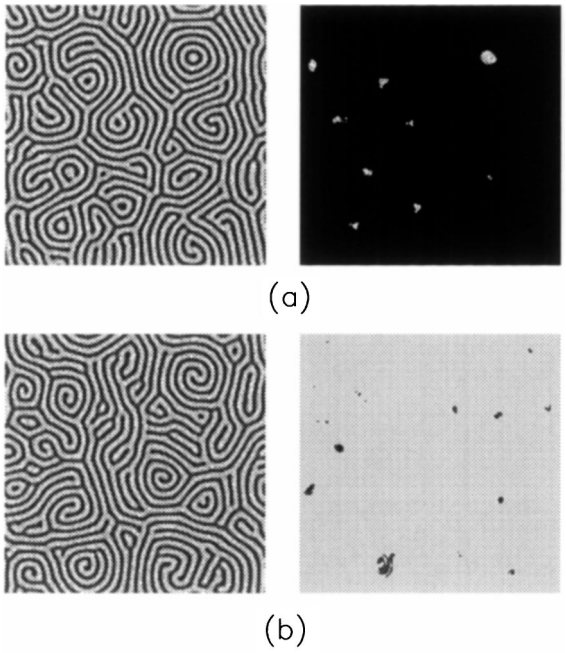

FIG. 1. Convective pattern (left) and mean flow (right) filtered by the condition $|\Psi| > \sup|\Psi|/3$ for rigid boundary conditions, $P = 1.2$, $\epsilon = 0.7$, and $\tau = 10$ (a) or $\tau = -10$ (b) showing positive and negative vortices according to sign(τ).

spatiotemporal chaotic dynamics governed by the propagation of dislocation arrays separating randomly oriented roll patches [Fig. 2(d)] whose size decreases as ϵ increases [23–25].

In order to quantitatively characterize the relaminarization effect of a moderate rotation, we have considered the

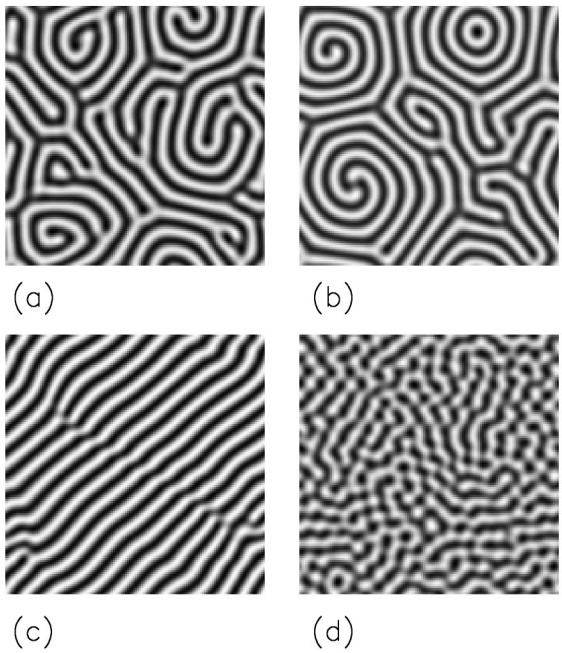

FIG. 2. Convective pattern for rigid boundary conditions at $P = 1.2$, $\epsilon = 0.7$, and rotation rates $\tau = 0$ (a), $\tau = 10$ (b), $\tau = 40$ (c), and $\tau = 56$ (d), to be compared to $\tau_{\mathrm{KL}} = 29.6$.

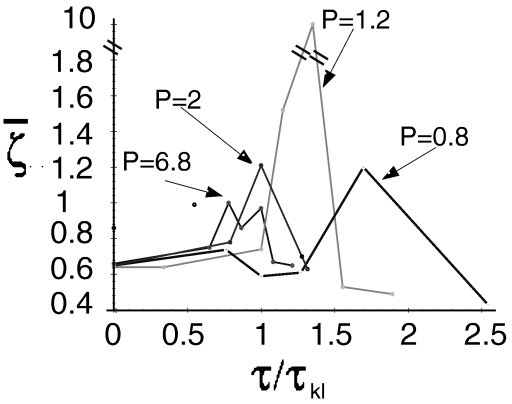

FIG. 3. Variation of the correlation length ζ with τ/τ_{KL}, for different values of the Prandtl number.

correlation length $\bar{\zeta}$, defined as the time average of $\zeta = (\langle k^2\rangle - \langle k\rangle^2)^{-1/2}$, where $\langle u\rangle$ stands for $\int u|\hat{W}(\vec{k})|^2 d^2\vec{k}/\int |\hat{W}(\vec{k})|^2 d^2\vec{k}$, and where $\hat{W}$ denotes the horizontal Fourier transform of the convective mode. Figure 3 displays the variation of $\bar{\zeta}$ with τ/τ_{KL} for different values of the Prandtl number. The relaminarization effect at small Prandtl number is clearly visible as a sharp maximum of the correlation length. This effect is also visible in experimental results reported in Fig. 4 of Ref. [26], although the authors do not stress this point. The maximum correlation occurs near τ_{KL} for Prandtl numbers larger than unity, but is associated to faster rotations when the Prandtl number is reduced. This indicates that rotation and mean flow act in opposite directions.

In a cylindrical geometry, the dislocations cannot annihilate each other as efficiently as in the periodic case. As a result, although the patterns obtained for intermediate values of the rotation rate [Fig. 4(b)] still present a higher degree of correlation than in the absence of rotation, they do not reduce to straight rolls. A noticeable feature is also that the patterns globally rotate (even when the rotation rate is smaller than $\tau_{\mathrm{KL}} = 23.6$ for $P = 0.8$), under the effect of dislocations generated on the boundary, an effect already noticed in laboratory experiments [27]. For $\tau > \tau_{\mathrm{KL}}$, the rolls tend to break under the effect of shear layers developed by the mean flow [Figs. 4(c) and 4(d)].

In the case of free-slip boundary conditions, the above dynamics is affected by the presence of the small-angle instability which is accurately reproduced when the three terms involving Ψ in $\mathcal{N}(W,\Psi)$ are retained. In the weakly nonlinear regime, the effect of this instability is to gradually rotate the convective rolls through reconnections of dislocations produced by the shearing motion of the mean flow.

In the fully nonlinear regime at moderate Prandtl number ($\epsilon = 0.5$, $P = 2$), the dynamics is significantly different from that obtained with rigid boundaries. In the absence of rotation, targets and spirals still form [Fig. 5(a)] but their coherence time is much shorter. The evolution is strikingly similar to that observed in laboratory experiments

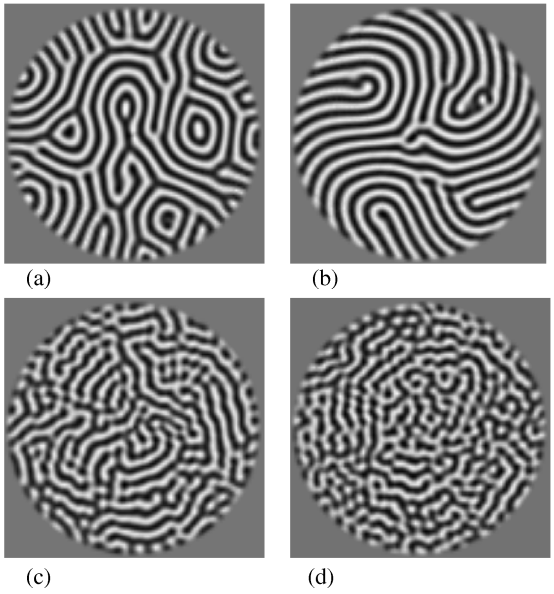

FIG. 4. Convective pattern in cylindrical geometry for $P = 0.8$, $\epsilon = 0.7$, and $\tau = 0$ (a), $\tau = 18$ (b), $\tau = 40$ (c), and $\tau = 60$ (d).

performed at a very large aspect ratio [14]. In both situations, the target formation is initiated by a defect instability, leading to "roll bulging, pinching and bridging" [28]. This suggests that the strength of the mean flow (which is weaker with rigid than with no-slip boundaries) can in fact be enhanced by increasing the aspect ratio of the container. With a small rotation ($\tau = 10$), targets of moderate size [Fig. 5(b)], associated to patches of positive vorticity

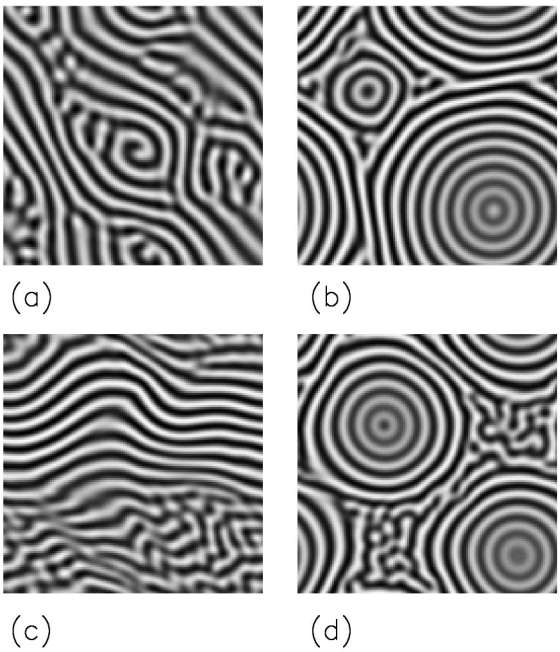

FIG. 5. Convective pattern for free-slip boundary conditions at $P = 2$, $\epsilon = 0.5$, with rotation rates $\tau = 0$ (a), $\tau = 10$ (b), and $\tau = 20$ taken at two different times (c),(d).

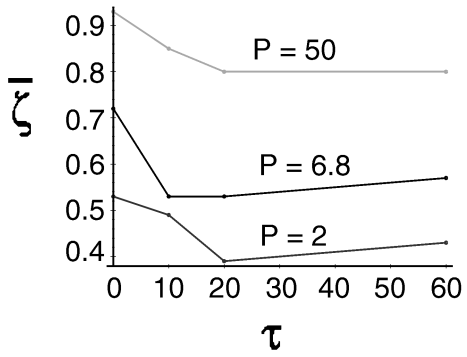

FIG. 6. Variation of the correlation length ζ with τ in the case of free-slip boundaries for different Prandtl numbers.

for the mean flow, are rapidly formed. They subsequently grow by accreting adjacent rolls and by merging together, leading to a unique coherent structure occupying the whole domain. At a larger value of the rotation rate ($\tau = 20$), the dynamics displays an early chaotic phase followed by the emergence of almost straight rolls, visible in the upper half of Fig. 5(c). Under the action of the small-angle instability, this structure, similar to that observed in the case of no-slip boundaries, is destabilized. It bends and progressively evolves towards big targets embedded in a chaotic background as displayed in Fig. 5(d). In the case of a cylindrical box, the pattern adjusts to the symmetry of the container, leading to concentric rolls which occupy the whole domain. The formation of these coherent targets is consistent with the continuous rotation symmetry of the small-angle instability. For $\tau = 60$, the dynamics is dominated by the Küppers-Lortz instability. The coherent structures are destroyed and a fully chaotic regime develops. Similarly, when at moderate rotation ($\tau = 10$) the Prandtl number is increased, the coherent targets formed at small values of the rotation rate become transients at $P = 6.8$, and totally disappear at $P = 50$.

Although with free-slip boundaries, the system develops strong coherent structures, the correlation length displayed in Fig. 6 is significantly different from that obtained with rigid boundaries. It does not display a maximum, because of the presence of a fully turbulent background. Furthermore, the destabilizing effect of the mean flow is clearly reflected by the growth of the correlation length with the Prandtl number, an effect emphasized by the free-slip boundaries.

T. P. acknowledges the hospitality of the Arizona Center for Mathematical Sciences. Part of this work has been supported by Contract No. AFOSRF49620-94-1-0463 and by the European Cooperative Network ERBC HRXCT930410. Numerical simulations were performed on the CRAY-C98 of IDRIS, Palaiseau.

[1] F. H. Busse and K. E. Heikes, Science **208**, 173 (1980).
[2] G. Küppers and D. Lortz, J. Fluid Mech. **35**, 609 (1969).
[3] R. M. Clever and F. H. Busse, J. Fluid Mech. **94**, 609 (1979).
[4] G. Küppers, Phys. Lett. **32A**, 7 (1970).
[5] T. Clune and E. Knobloch, Phys. Rev. E **47**, 2536 (1993).
[6] Y. Ponty, T. Passot, and P. L. Sulem, Phys. Fluids **9**, 67 (1997).
[7] F. H. Busse and E. W. Bolton, J. Fluid Mech. **146**, 115 (1984).
[8] Y. Tu and M. C. Cross, Phys. Rev. Lett. **69**, 2515 (1992).
[9] Y. Ponty, T. Passot, and P. L. Sulem, "Pattern Dynamics in Rotating Convection at Finite Prandtl Number" (to be published).
[10] S. Chandrasekhar, *Hydrodynamic and Hydromagnetic Stability* (Oxford University Press, New York, 1961).
[11] P. Manneville, J. Phys. (Paris) **44**, 759 (1983).
[12] Haowen Xi, J. D. Gunton, and G. A. Markish, Physica (Amsterdam) **204A**, 741 (1994).
[13] S. W. Morris, E. Bodenschatz, D. S. Cannell, and G. Ahlers, Phys. Rev. Lett. **71**, 2026 (1993).
[14] M. Assenheimer and V. Steinberg, Phys. Rev. Lett. **70**, 3888 (1993).
[15] W. Decker, W. Pesch, and A. Weber, Phys. Rev. Lett. **73**, 648 (1994).
[16] Y. Hu, R. Ecke, and G. Ahlers, Phys. Rev. E **51**, 3263 (1995).
[17] J. Liu and G. Ahlers, Phys. Rev. Lett. **77**, 3126 (1996).
[18] M. Cross, Physica (Amsterdam) **97D**, 65 (1996).
[19] Haowen Xi and J. D. Gunton, Phys. Rev. E **52**, 4963 (1995).
[20] R. E. Ecke, Y. Hu, R. Mainieri, and G. Ahlers, Science **269**, 1704 (1995).
[21] J. Millán-Rodríguez, M. Bestehorn, C. Pérez-García, and R. Friedrich, Phys. Rev. Lett, **74**, 530 (1995).
[22] J. Millán-Rodríguez and C. Pérez-García, Chaos **4**, 369 (1994).
[23] M. Neufeld, R. Friedrich, and H. Haken, Z. Phys. B **92**, 243 (1993).
[24] M. Fantz, R. Friedrich, M. Bestehorn, and H. Haken, Physica (Amsterdam) **61**, 147 (1992).
[25] M. C. Cross, D. Meiron, and Y. Tu, Chaos **4**, 607 (1994).
[26] Y. Hu, R. E. Ecke, and G. Ahlers, Phys. Rev. Lett. **74**, 5040 (1995).
[27] F. Zong, R. Ecke, and V. Steinberg, Physica (Amsterdam) **51D**, 596 (1991).
[28] M. Assenheimer and V. Steinberg, Nature (London) **367**, 345 (1994).